Supporting Information for

# FRET from Multiple Pathways in Fluorophore Labeled DNA

*Joseph S. Melinger[1,*], Ani Khachatrian[1], Mario G. Ancona[1], Susan Buckhout-White[3], Ellen R. Goldman[3], Christopher M. Spillmann[3], Igor L. Medintz[3], and Paul D. Cunningham[1]*

[1]Electronics Science and Technology Division, Code 6800, U.S, Naval Research Laboratory, Washington, DC 20375

[2]Sotera Defense, 430 National Business Parkway, Suite 100, Annapolis Junction, Maryland 20701

[3]Center for BioMolecular Science and Engineering, Code 6900, U.S, Naval Research Laboratory, Washington, DC 20375

## DNA oligo sequences and structure of fluorophores and linkers

Base sequences
DR1: ACACGAGTTGATGCACTAAGTGCGGCACGGCTAGTT
DR2: /Cy3/TTCGTTCCCTACAGGGTGAT/Cy3/
DR3: /Cy3.5/TACGACGCAGAACGAGCGAATT/Cy3.5/
DR4: GAGTAGGACAACGTCCAGTT
DR5: TACCCACACTAAGTCACGGGAT
DRTemp1: TAGTGTGGGTATGTCCTACTCTCTGCGTCGTAAGGGAACGAATAGTGCATCAACTCGTGT
DRTemp2: AACTAGCCGTGCCGCACTATCACCCTGTAATTCGCTCGTAACTGGACGTATCCCGTGACT

a)

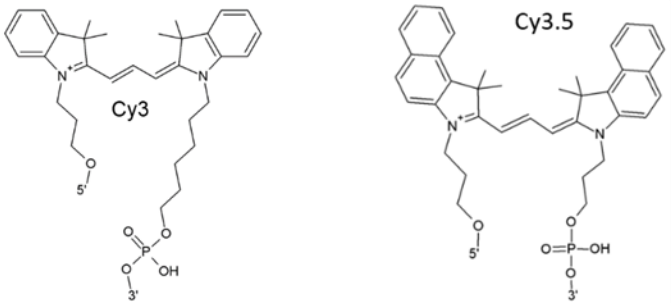


b)

**Fig. S1** a) The nucleobase sequences for each oligo. b) Chemical structures for the Cy3 and Cy3.5 fluorophores. The Cy3 is attached via a 3C linker on the 5' end and a 6C linker on the 3' end. The Cy3.5 uses the 3C linker for both attachments.

## Electrophoresis and Formation Efficiency

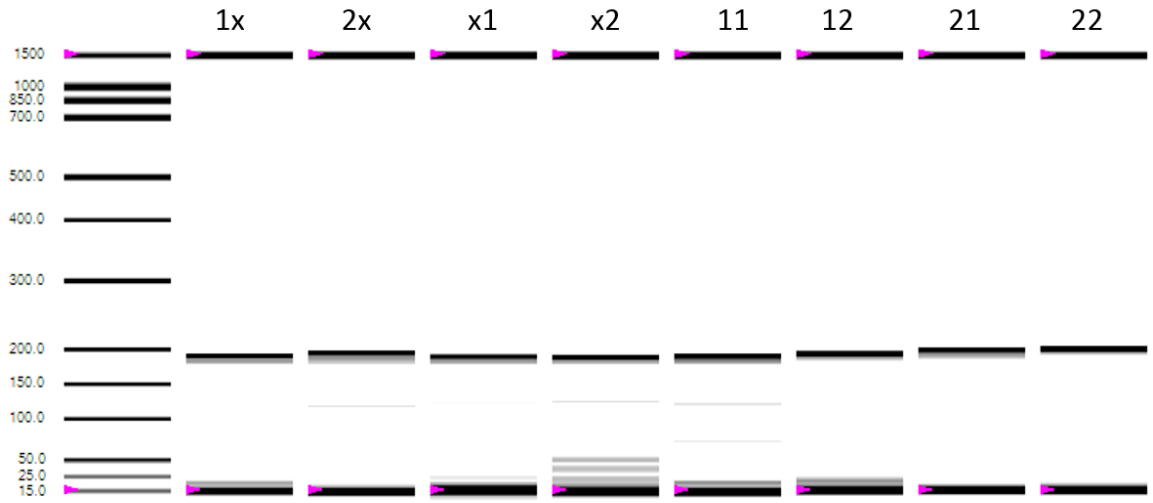


| Structure | % unformed structures | % partial structures | % full structures |
|---|---|---|---|
| **1x** | 34 | 6 | 59 |
| **2x** | 10 | 14 | 76 |
| **x1** | 34 | 10 | 56 |
| **x2** | 35 | 20 | 45 |
| **11** | 30 | 20 | 50 |
| **21** | 8 | 17 | 75 |
| **12** | 33 | 18 | 49 |
| **22** | 12 | 18 | 70 |
| Avg. | 25 | 15 | 60 |

**Fig. S2.** Top: Electrophoresis of dual rail FRET structures and control structures. The left most column is the separation of DNA containing known number of base pairs. Bottom: Analysis in terms of the percentage of unformed, partially formed, and fully formed structures. The average formation across all structures is also given.

Formation Efficiency was calculated through use of microfluidic automated electrophoresis on a Bio-Rad Experion system. 1μL of sample was placed into a DNA 1K analysis chip and analyzed on the Experion software. For purposes of formation calculations based on the expected final base pair size of the structure, greater than 180bp was considered fully formed, less than 40bp was considered unformed and a band in the middle of those ranges were considered partially formed. All samples were evaluated and averaged for a formation yield of 60% formed and 25% unformed.

## Absorption spectra and fluorescence excitation profiles of control structures

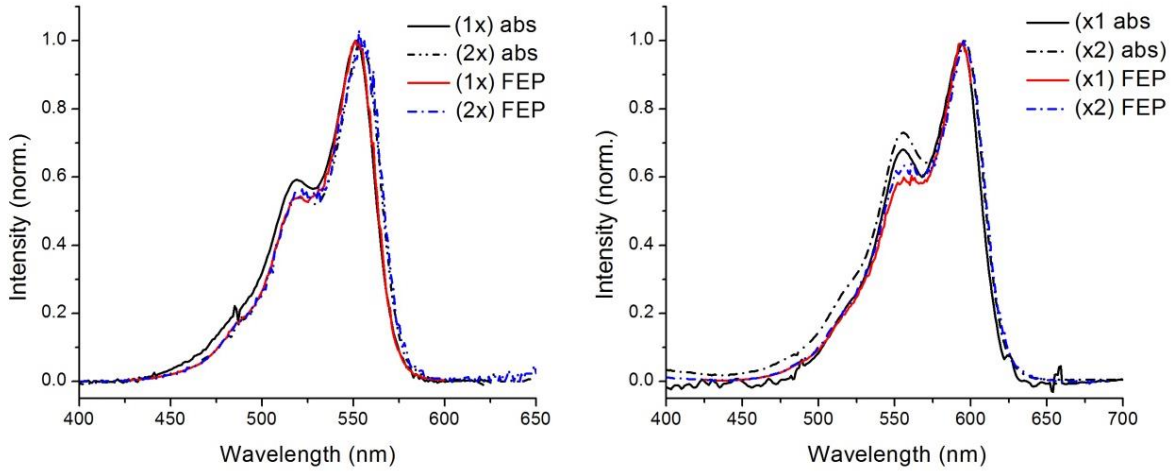


**Fig S3**. Left Panel: Absorption spectra and corresponding fluorescence excitation profiles (FEPs) for control structures **1x** and **2x**. The detection wavelength was 660 nm for the FEP. Right Panel: Absorption spectra and corresponding FEPs for control structures **x1** and **x2**. The detection wavelength was 710 nm for the FEP.

## Fluorescence decay dynamics of control structures

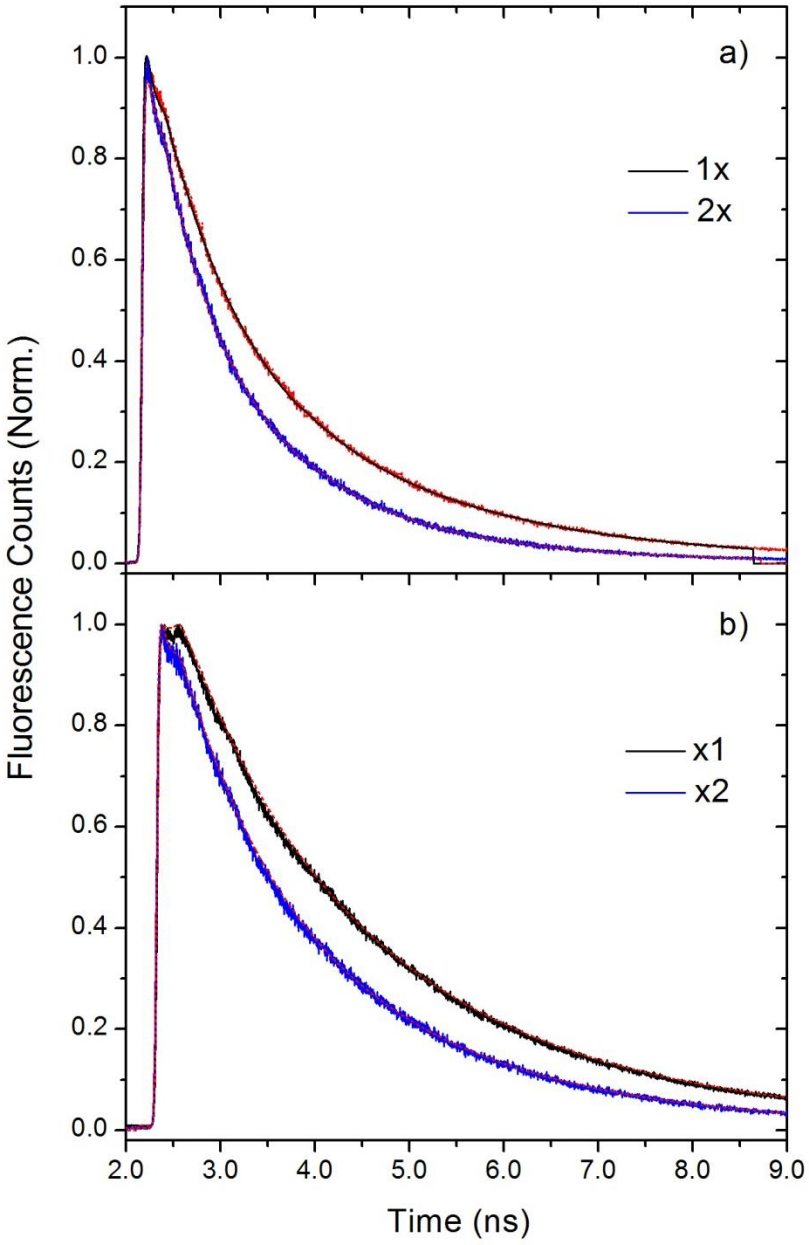


**Fig. S4**. Excited state fluorescence decay dynamics as measured by time-correlated single photon counting (TCSPC) for donor-only and acceptor-only controls. The excitation wavelength is 532 nm. a) Fluorescence decays for control structures **1x** and **2x**. b) Fluorescence decays for control structures **x1** and **x2**. In both panels the red lines are fits to the data using a sum of three exponential decay functions. The average lifetimes are given in Table S1.

**Ultrafast Anisotropy Dynamics from Homo-FRET**

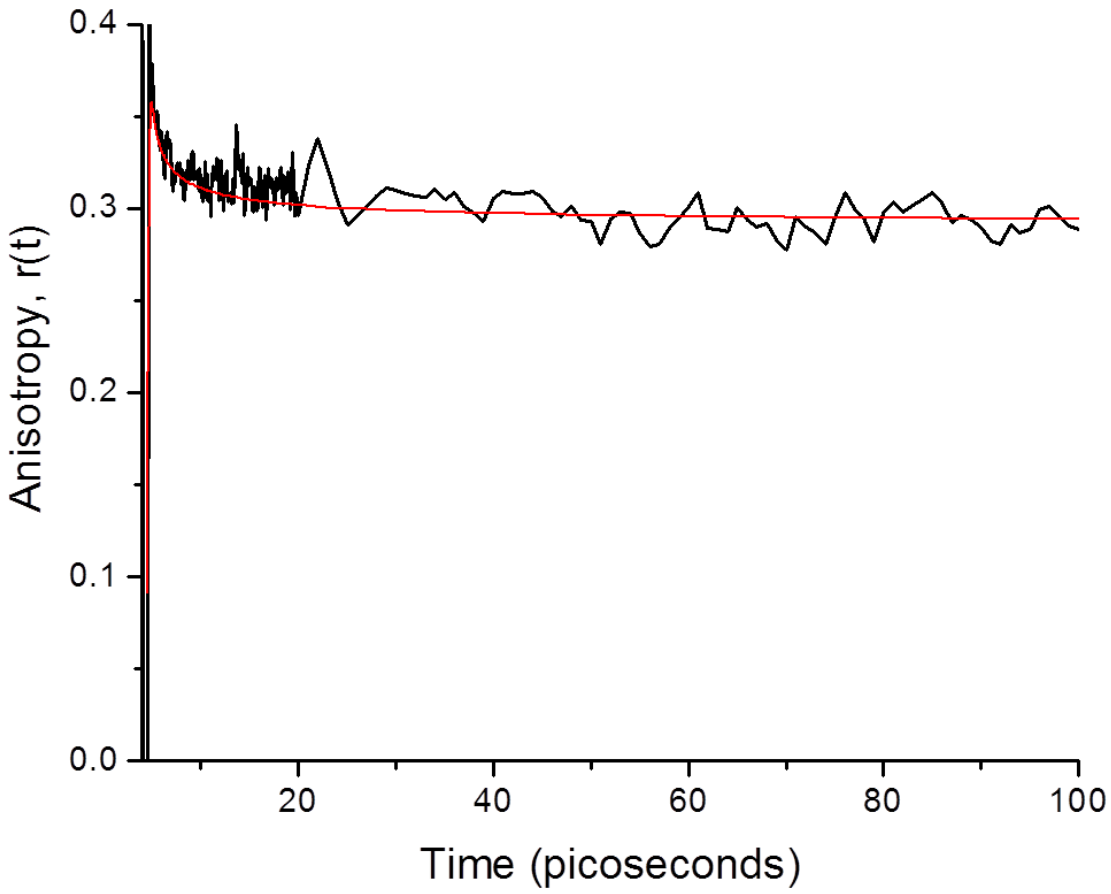


**Fig. S5**. Time resolved anisotropy of the dual rail control structures **2x**. The red line is a simulation of the experiment based on a Monte Carlo simulation described below. The initial decay is approximately 1.5 picoseconds corresponding to a 13 Å separation between Cy3 fluorophores.

The time resolved anisotropy decay for the structure **2x** was determined by ultrafast pump-probe spectroscopy using

$$r(t) = \frac{I_{\parallel} - I_{\perp}}{I_{\parallel} + 2I_{\perp}}, \qquad \text{(S1)}$$

Where $I_{\parallel}$ and $I_{\perp}$ are the transient bleach signals (ΔT/T) with the probe pulse polarized parallel and perpendicular, respectively, to the pump beam. Here, the pump pulse was tuned to 520 nm

and the probe pulse was tuned to 555 nm. The Monte Carlo simulation was based on Eq. 9 of the main text simplified to a system of two donor fluorophores, or

$$\begin{aligned}\frac{dD_1^{(i)}(t)}{dt} &= -(K_D + K_{\mathrm{hom}}^{(i)})D_1^{(i)}(t) + K_{\mathrm{hom}}^{(i)}D_2^{(i)}(t) \\ \frac{dD_2^{(i)}(t)}{dt} &= -(K_D + K_{\mathrm{hom}}^{(i)})D_2^{(i)}(t) + K_{\mathrm{hom}}^{(i)}D_1^{(i)}(t)\end{aligned} \qquad \text{(S2)}$$

where $D_1$ and $D_2$ represent the probabilities of the donor fluorophores being excited, $K_D$ is the excited state inverse lifetime of the donor, and $K_{\mathrm{hom}}$ is the rate constant for homo-FRET between the two donors.

$$K_{\mathrm{hom}}^{(i)} = K_D\left(\frac{R_0^{(i)}}{r_{D_1D_2}}\right)^6 \qquad \text{(S3)}$$

where $r_{DD}$ is the donor-donor distance, and $R_0^{(i)}$ is the Förster radius of the interaction. In Eqs. S2 and S3 the superscript *i* labels the member of the ensemble having a particular arrangement of orientations. The solution to S2 yields the time evolution of the donor excited states. For the case that the donor labeled $D_1$ absorbs a photon, we arrive at

$$\begin{aligned}D_1^{(i)}(t) &= \frac{1}{2}e^{-K_D t}\left(1 + e^{-2K_{\mathrm{hom}}^{(i)}t}\right) \\ D_2^{(i)}(t) &= \frac{1}{2}e^{-K_D t}\left(1 - e^{-2K_{\mathrm{hom}}^{(i)}t}\right)\end{aligned}. \qquad \text{(S4)}$$

Adding the two contributions to the donor dynamics, we see that the homo-FRET term cancels so that homo-FRET does not change the observed donor lifetime. The anisotropy decay is found by setting the donor decay rate to 0 and multiplying $D_1$ by the initial donor anisotropy, $r_0 = 0.4$,

$$r(t) = \frac{r_0}{2}\left(1 + e^{-2K_{\mathrm{hom}}^{(i)}t}\right). \qquad \text{(S5)}$$

This gives the depolarization of the photoexcited donor due to homo-FRET and is equivalent to the analysis used by Berberan-Santos and Valeur[1]. Each member of the ensemble of randomly oriented dyes contributes a different homo-FRET rate to Eqn S5 and generates its own *r(t)*. These are summed and normalized by the number of initially photoexcited donors. Given the fast rate of homo-FRET, the simulated anisotropy is convolved with a 200 fs Gaussian to account for the instrument response function. Good agreement to the measured anisotropy is found for a donor separation of 13 Å. It is clear that ~100% energy transfer will cause the anisotropy to decay to $\sim r_0/2$, however, the anisotropy of **2x** only decays to 0.3. The fast anisotropy dynamics imply that a larger donor separation cannot be used to explain this discrepancy. Instead, the data suggests that nearly half of the population does not depolarize through homo-FRET, and instead contribute a constant $r_0$ over time-scales relevant to FRET. Formation errors may contribute here, yielding structures that do not undergo homo-FRET. Interactions between a portion of the closely spaced donors in the ensemble may lead to molecular exciton formation, which could explain the reduced quantum yields of **2x** as compared to **1x**. Also, the motion of the two donors may be somewhat correlated so that their relative dipole orientations are not random, yielding incomplete depolarization.

**Monte Carlo simulation of the orientation factor $\kappa^2$ in the static isotropic limit**

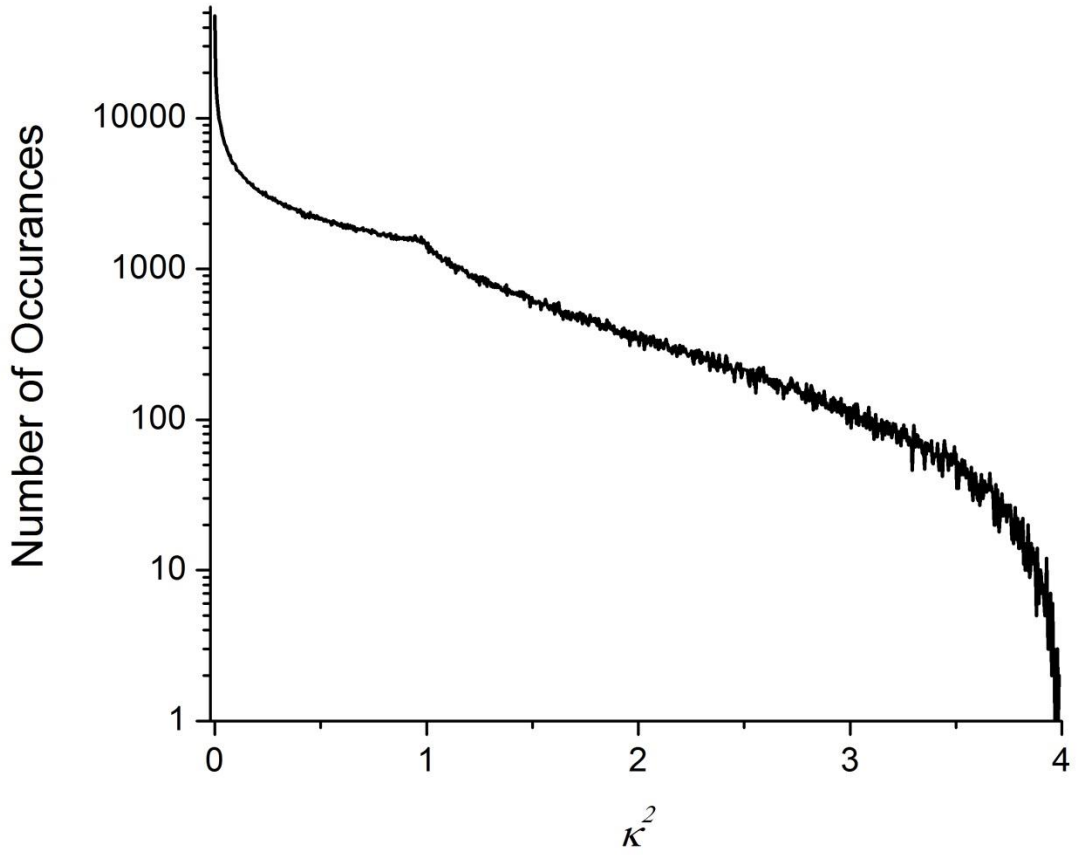


**Fig. S6**. Monte Carlo simulation of the orientation factor $\kappa^2$ assuming a static isotropic distribution of transition dipoles. Here, the angles θ and ω are taken to be randomly distributed. The graph represents the results of 1,000,000 choices of θ and ω generated by a random process.

**Simulation of FRET efficiency increase resulting from a second donor and/or acceptor**

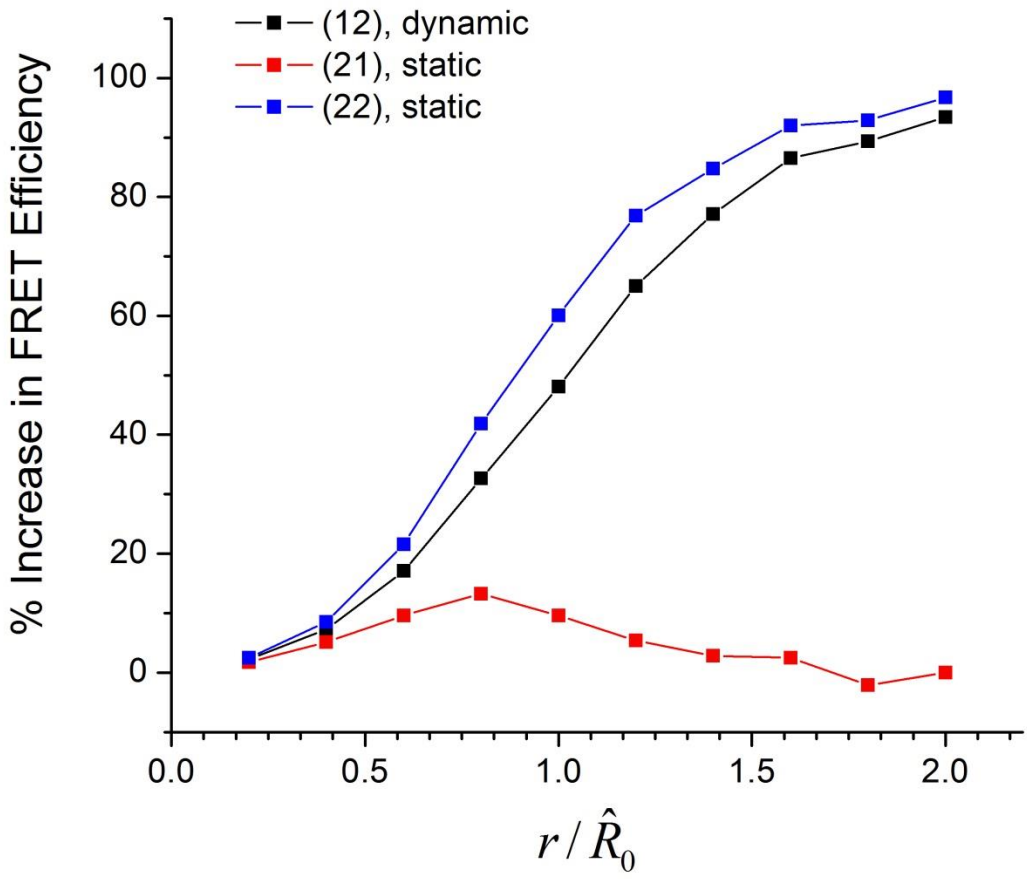


**Fig. S7**. Plots of the percentage increase in FRET efficiency for multi-fluorophore labeled structures versus the normalized separation distance, $r/\hat{R}_0$. The percentage increase in FRET efficiency is referenced to the FRET efficiency of structure **11** through $\frac{E_{ij} - E_{11}}{E_{11}} \times 100\%$, where $E_{ij}$ corresponds to the FRET efficiency of structures **21**, **12**, and **22**.

Table S1. Optical and photophysical properties of donor and acceptor controls and the construct **11**.

| **Construct** | **QY**[a] | **$\langle\tau\rangle$**[b] **(ns)** | **Ext. Coeff**[c] **($M^{-1}cm^{-1}$)** | **$\lambda_{max,abs}$ (nm)** | **$\lambda_{max,em}$ (nm)** | **$\lambda_{max,FEP}$ (nm)** | **J**[d] **$M^{-1}cm^{-1}nm^4$** | **$\hat{R}_0$**[e] **(Å)** |
|---|---|---|---|---|---|---|---|---|
| **1x** | 0.37 (0.03) | 1.2 | 150,000 | 552 | 565 | 552 | - | - |
| **2x** | 0.25 (0.02) | 0.95 | - | 554 | 567 | 553 | $3.8x10^{15}$ | 52 (1) |
| **x1** | 0.42 (0.04) | 2.0 | 150,000 | 595 | 610 | 593 | - | - |
| **x2** | 0.31 (0.04) | 1.4 | - | 595 | 612 | 595 | - | - |
| **11** | - | - | - | 552 | 565 | 552 | $7.0x10^{15}$ | 59 (1) |

[a]Fluorescence quantum yield. Values in parenthesis represent the standard deviation based on three measurements.

[b]Average fluorescence lifetime determined from fitting to a sum of exponential decay terms

[c]Molar extinction coefficient. Values taken from Ref. 5 of main text.

[d]Spectral Overlap Integral calculated from Eq. 2 of main text.

[e]Förster radius for the case of $\kappa^2 = 2/3$. Values in the parenthesis represent the propagated error based on the uncertainty in QY.

Table S2. Donor fluorescence decay parameters for one sample set.

| | $A_1$ | $\tau_1$ (ns) | $A_2$ | $\tau_2$ (ns) | $A_3$ | $\tau_3$ (ns) | $\tau_{av}$ |
|---|---|---|---|---|---|---|---|
| **1x** | 2277 | 0.086 | 6574 | 0.73 | 6216 | 2.10 | 1.20 |
| **x1** | 3193 | 0.79 | 13130 | 2.35 | - | - | 2.04 |
| **2x** | 2430 | 0.27 | 5125 | 0.92 | 1704 | 1.96 | 0.95 |
| **x2** | 1011 | 0.061 | 3187 | 0.81 | 4995 | 2.10 | 1.43 |
| **11** | 7426 | 0.11 | 5646 | 0.54 | 2064 | 1.97 | 0.52 |
| **21** | 6358 | 0.075 | 2815 | 0.43 | 919 | 1.72 | 0.32 |
| **12** | 13156 | 0.058 | 3846 | 0.49 | 1831 | 2.0 | 0.33 |
| **22** | 16231 | 0.049 | 3362 | 0.37 | 1162 | 1.73 | 0.20 |

The donor decay was fit to a tri-exponential function of the form $A_1\exp(-t/\tau_1) + A_2\exp(-t/\tau_2) + A_3\exp(-t/\tau_3)$ where the $A_i$ are amplitudes and $\tau_i$ are lifetimes. The fit was performed using the Floufit package (Picoquant) with convolution of the instrument response function (~ 45 ps at the FWHM). From the fitting the FRET efficiencies (E) are estimated using Eq. 7 of the main text.

**Monte Carlo Simulations of FRET Dynamics**

The FRET dynamics were modeled using Monte Carlo simulations of an ensemble of FRET networks of static fluorophores whose orientations were allowed to vary isotropically[2]. Each member of the ensemble consisted of two to four fluorophores, and between 1 and 5 FRET pathways, depending on the construct being modeled. The angles $\theta$ and $\omega$ are sufficient to define the relative dipole orientations for each pair-wise FRET interaction. Here $\theta$ is the angle between the donor transition dipole moment and the vector pointing from the center of the donor to the center of the acceptor, and $\omega$ is the angle between the acceptor transition dipole moment and the electric dipole field associated with the donor at the location of the acceptor (Eq. 8 in the main text). For each FRET pathway, these angles were randomly chosen from isotropic distributions as $Cos\theta \in [-1,1]$. The orientation factor $\kappa^2$ of each FRET interaction was found by applying Eq. 8 to each choice of angles. Independently, each pair-wise FRET interaction shows the characteristic $\kappa^2$ distribution associated with static isotropic transition dipole orientations, Fig. S6.

The FRET rates were calculated for each FRET pathway based solely on the separation between fluorophores. We take the separation between donors to be 13Å (based on the homo-FRET measurement of Fig. S5) and the intitial donor-acceptor separation to be 34 Å. The FRET rates were then input into the system of differential equations that describe energy transfer dynamics in the FRET network, e.g. Eq. 9 of the main text for **22**. The system of equations is solved in matrix form as an Eigenvalue problem using Wolfram Mathematica. The solutions are the time-dependent population dynamics for each process, e.g. $D_1(t)$, $D_2(t)$, and $A(t)$ for the case where $D_1$ is initially photoexcited. The contributions from photoexcitation of both donors must be considered, as they are indistinguishable. Since we seek to model dilute solutions that are photoexcited at low fluence, we do not consider the case of both donors being photoexcited simultaneously. The solutions are summed for all members of the ensemble for each FRET process. The simulation of the donor decay and acceptor rise dynamics are performed while varying the donor-acceptor distance from the starting value of 34 Å.

It bares mention that we do not consider homo-FRET between acceptors. This is not needed, since homo-FRET out of one acceptor is perfectly balanced by homo-FRET in from the other acceptor. In this way, the observed acceptor decay remains unchanged in the presence of homo-FRET. However, dynamic quenching due to interactions between proximal dyes may reduce the observed lifetime.

Direct excitation of the acceptor was accounted for by considering the dynamics of *A(t)* for initial photoexcitation of the acceptor and adjusting the weight of each term by the relative absorption of the donor and acceptor at the pump wavelength. We also consider the effects of cross-talk, defined here as the unavoidable detection of dynamics associated with a different fluorophore than the one intended. In fluorescence experiments, this can arise when the tail of the donor emission spectrum overlaps with the emission spectrum of the acceptor. The situation is further complicated for pump-probe measurements, where the ground-state bleach of the acceptor can also overlap with the ground-state bleach of the donor. We accounted for cross-talk by adjusting each contribution to the population dynamics at a given wavelength by the relative amplitude of the ground state bleach of each fluorophore observed in transient absorption spectra.

The FRET efficiency distribution for each ensemble is found by setting the acceptor decay rate $K_A$ to zero so that at long delays after FRET is complete, e.g. 10 ns, the calculated acceptor dynamics saturate to the FRET probability for each member of the ensemble. This FRET probability is simply the FRET efficiency considered for a single excitation event. This method implicitly includes multiple homo-FRET events between the donors because back-transfer is included in the differential equation. The FRET efficiency distributions for **11, 12**, **21,** and **22**, are shown in Fig. 5 along with the ensemble average efficiency for each.

**References.**

(1) Berberan-Santos, M. N.; Valeur, B., Fluorescence depolarization by electronic energy transfer in donor-acceptor pairs of like and unlike chromophores. *J. Chem. Phys.* **1991,** 95, 8048-8055.

(2) Vogel, S. S.; van der Meer, B. W.; Blank, P. S., Estimating the distance separating fluorescent protein FRET pairs. *Methods* **2014,** 66, 131-138.